Flow-destabilized seiche modes with a movable dam

Hélène Scolan

August 2009

1 Introduction

Volcanic tremors are seismic signals emanating from fluid channels encased in rock. The understanding of the mechanism of this phenomenon is of great importance to improve evaluation of volcanic eruptions. Many possibilities have been advanced to understand the mechanism responsible for these low-frequency signals.

It has been suggested recently [5] that the seismicity could be the result of flow-destabilized oscillations whose frequency is set by an adjacent reservoir in the rock. Thus, the channel in the rock would act like a clarinet reed exciting and interacting with standing waves in an adjacent reservoir (Fig 1).

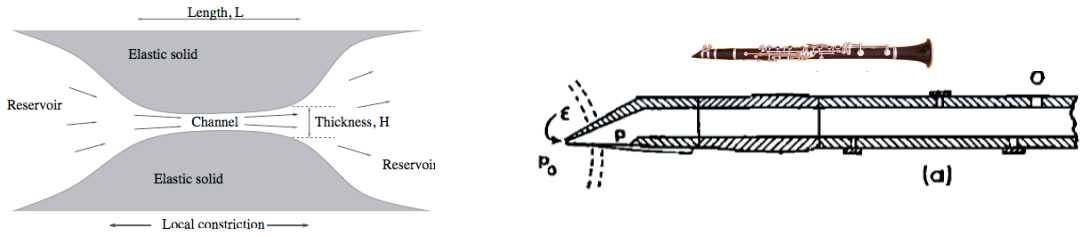

Figure 1: Oscillating reed in a clarinet (Backus 1963 [1]) or rock excitating and interacting with standing waves in the adjacent reservoir [5].

In the musical instrument, the sound is produced thanks to an instability arising from the coupling between the flow in the reed and the feedback from the resonating cavity. In the same way, crack or 'sloshing' modes (instead of acoustic modes) in a reservoir adjacent to a channel in the rock could be the relevant mechanism of generation of the low-frequency seismicity in volcanic tremor.[5]

So far, the theory of destabilized sloshing modes has not been deeply studied. The purpose of this project is to explore and illustrate the mechanism using a simple analogous laboratory configuration involving water instead of magma and looking for flow-destabilized seiche modes (Fig 2).

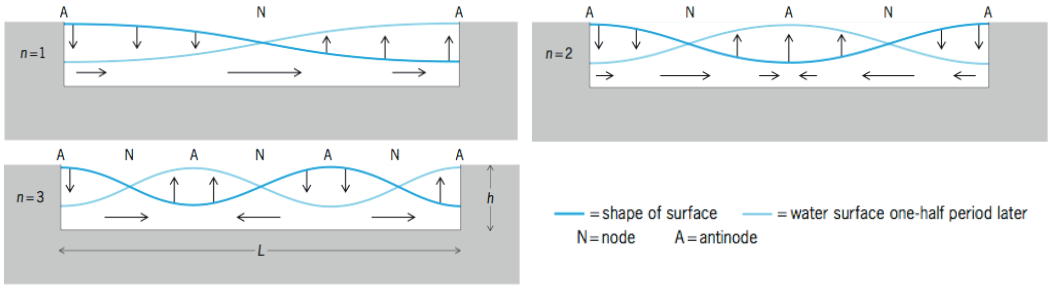

Figure 2: Seiches modes in a box: standing waves with $T = \frac{2L}{n\sqrt{gh}}$

2 Experiment in water : a reservoir and a movable dam

Figure 3 illustrates the experimental setup chosen to investigate the phenomenon. It looks like a clarinet in that a movable plexiglas plate (the "paddle") plays the role of the reed in the instrument and there is an adjacent reservoir. Water flows at constant flow rate into the reservoir. The plexiglas plate attached to a pivoted rod and masses are first added at the other extremity in order to counterbalance the weight of the plate. A addtional mass m_{added} is then put at varying positions x on the rod to make the plate go down.

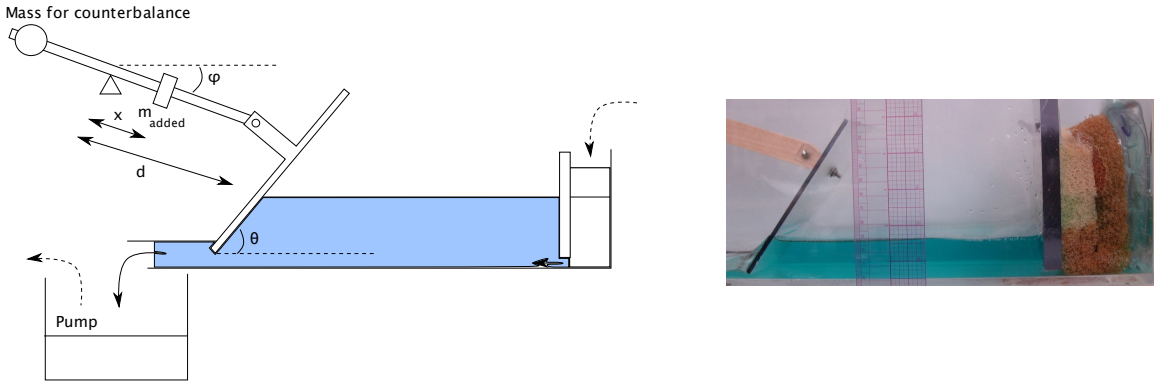

Figure 3: Experimental setup: the reservoir length is around 20 cm, d=50cm. m_{added} varies from 3 to 100g and the height of water can vary from around 2 cm to 5 cm.

Blue dye is added in the water to enhance the contrast in the images taken at 15 fps with a Pulnix camera. Turbulence near the inflow to the reservoir is prevented by inserting a sponge or polystyrene foam. However, as that dampening structure also absorbs waves, a plexiglas barrier is placed in front to promote wave reflections.

First, the goal will be to understand theoretically under what conditions the instability appears and then to observe the phenomenon experimentally.

3 A shallow water model

3.1 Governing equations

3.1.1 Equation for the paddle

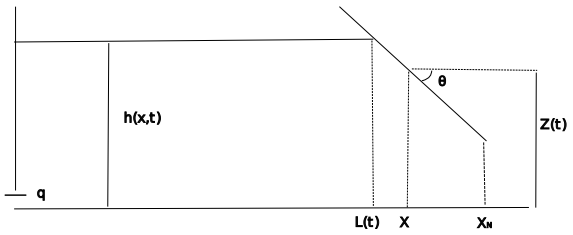

Figure 4: Diagram of the system and notations.

The motion of the paddle is described by the conservation of angular momentum applied on the pivot point (triangle in figure 3):

$$J\ddot{\phi} = -mgd\cos(\phi) + F\cos(\phi) \tag{1}$$

where J is the moment of inertia, that can be written as $J = (M+m)d^2$, with a global effective mass M and an additional equivalent mass m placed on the end on the paddle. (i.e. m is linked to the excess mass added on the paddle by $m_{\text{added}}x^2 = md^2$).

We consider here only the force due to the gravity and F, the vertical force of the water on the paddle. Friction (for example in the hinge) is neglected. The force F is essentially the vertical component of the normal pressure force (dominating drag force) exerted on the paddle by the fluid. Introducing W, the transversal width of the reservoir, we have therefore:

$$J\ddot{\phi} = -mgd\cos(\phi) + Wd\cos(\phi)\cos\theta\int_L^{X_N} p dx \tag{2}$$

If ϕ is a small angle, $\cos(\phi) \approx 1$ and the position $Z(t)$ of the paddle satisfies: $\dot{Z}(t) \approx d\dot{\phi}(t)$ then the governing equation of the paddle is finally:

$$(m+M)\ddot{Z} = -mg + W\cos\theta\int_L^{X_N} p dx \tag{3}$$

3.1.2 Equations in the fluid

We will work here with an inviscid shallow water model (assuming the height remains smaller than the horizontal scale). The problem can be divided up into two regions:

• For $x > L$, the water flows underneath the paddle, and the height and velocity satisfy the following equations:

$$h = Z(t) + (X - x)\tan\theta \tag{4}$$

$$h_t = \dot{Z} = -(hu)_x \tag{5}$$

$$u_t + uu_x = -\frac{p_x}{\rho} \tag{6}$$

where u_i is the derivative of u with respect to i. X is the position of the middle of the paddle and $Z(t)$ its vertical position. The boundary conditions specify the continuity of the flow velocity and height at $x = L$:

$$u(x \to L^-) = u_L \tag{7}$$
$$h(x \to L^-) = h_L = Z + (X - L)\tan\theta \tag{8}$$

Equation (5) can be integrated between L and x to give an expression for the velocity:

$$u = \frac{h_L u_L + (L - x)\dot{Z}}{Z + (X - x)\tan\theta}$$

• For $0 < x < L$, the water surface is free, implying a hydrostatic pressure, and we have:

$$h_t + (hu)_x = 0 \tag{9}$$
$$u_t + uu_x = -gh_x \tag{10}$$
$$\tag{11}$$

The imposition of a constant flow rate q at $x = 0$, and the continuity at the right are written as:

$$[hu]_{x=0} = q \tag{12}$$
$$h(x = L) = h_L = Z + (X - L)\tan\theta \tag{13}$$

The problem contains three unknowns, $Z(t)$, $L(t)$ and $u_L(t)$, that are determined using the equation of motion of the paddle, the equations of the fluid for $0 < x < L$, and equation (6) integrated between $x = L$ and the end of the paddle, $x = X_N$, where we assume that the pressure becomes hydrostatic again: $-\int_L^{X_N}(u_t + uu_x)dx = \rho g(h_N - h_L)$.

3.2 Adimensionalisation

3.2.1 Scaling

In order to simplify the problem and uncover the important non-dimensional parameters, we consider different scalings for x in the two regions:

• For the reservoir, the natural scale for distance is X, the position of the paddle. So we use $\hat{x} = \dfrac{x}{X}$ for $0 < x < L$.

• Under the paddle, the relevant distance is $X_N - X$, so we introduce another variable ξ such that:

$$x = (X_N - X)\xi + X \tag{14}$$

with $l < \xi < 1$ where $l = \frac{L-X}{X_N-X}$. i.e.

$$\hat{x} = R\xi + 1$$

with the ratio, $R = \dfrac{X_N - X}{X}$

The vertical scale is set by $(X_N - X)\tan\theta$ so all the other non-dimensional quantities are written:

$$\hat{h} = \frac{h}{(X_N - X)\tan\theta}$$

$$\hat{u} = \frac{u}{\sqrt{g(X_N - X)\tan\theta}}$$

$$\hat{t} = \frac{t}{\frac{X}{\sqrt{g(X_N - X)\tan\theta}}}$$

$$\hat{p} = \frac{p}{\rho g(X_N - X)\tan\theta}$$

3.2.2 Adimensionalised equations

We then derive the adimensionalised form of the equations of the fluid:

• For $x > L$:

$$\hat{h} = \hat{Z} - \xi \tag{15}$$

$$\hat{h_t} = \dot{\hat{Z}} = -(\hat{h}\hat{u})_{\hat{x}} \tag{16}$$

$$\hat{p}_\xi = -\hat{u}\hat{u}_\xi - R\hat{u}_{\hat{t}} \tag{17}$$

with the boundary conditions:

$$\hat{u}_{\hat{L}} = u(\hat{x} = 1 + Rl) \tag{18}$$

$$\hat{h}_{\hat{L}} = h(\hat{x} = 1 + Rl) \tag{19}$$

$$\hat{u} = \frac{\hat{q_L}}{\hat{Z} - \xi} - R\frac{\xi - l}{\hat{Z} - \xi} \tag{20}$$

• For $0 < x < L$, it is convenient to write everything in terms of the flow rate $q = uh$ and the height h (instead of u and h):

$$\hat{h}_{\hat{t}} + \hat{q}_{\hat{x}} = 0 \tag{21}$$

$$\hat{q}_{\hat{t}} + (\frac{\hat{q}^2}{\hat{h}})_{\hat{x}} = -\hat{h}\hat{h}_{\hat{x}} \tag{22}$$

with the boundary conditions:

$$[\hat{h}\hat{u}]_{\hat{x}=0} = \hat{q} \tag{23}$$

$$\hat{h}_{\hat{L}} = h(\hat{x} = 1 + Rl) \tag{24}$$

The equation 3 for the paddle becomes:

$$I\ddot{\hat{Z}} = -1 + \mu \int_l^1 p d\xi \tag{25}$$

where I and μ are two dimensionless parameters.

3.2.3 Control parameters

We distinguish 5 parameters in the system:

- $I = \dfrac{m+M}{m} R^2 \tan^2\theta$ the inertia term,
- $\mu = \dfrac{\rho W (X_N - X)^2 \sin\theta}{m}$ corresponding to the ratio $\dfrac{\text{mass of water under the paddle}}{\text{mass on the paddle}}$
- $R = \dfrac{X_N - X}{X} = \hat{X}_N - 1$ the aspect ratio horizontally between the distance under the paddle and the length of the reservoir.
- $\hat{Q} = \dfrac{q}{\sqrt{g}((X_N - X)\tan\theta)^{3/2}}$ the dimensionless imposed flow rate.

3.3 Approximation for small R

To simplify the problem, we add the hypothesis that R is small, implying that the distance under the paddle is small compared to the length of the reservoir. Then, if we recall the equations for $x > L$:

$$\hat{u} = \frac{\hat{q_L}}{\hat{Z} - \xi} - R\frac{\xi - l}{\hat{Z} - \xi}$$
$$\hat{p}_\xi = -\hat{u}\hat{u}_\xi - R\hat{u}_{\hat{t}}$$
$$I\ddot{\hat{Z}} = -1 + \mu \int_l^1 p d\xi$$

We obtain $u \approx \dfrac{q_L}{Z - \xi} = \dfrac{q_L}{h}$ and $p_\xi \approx -u u_\xi$.
(Now we work with the non-dimensional variables and omit the hat in the formulas).

If we integrate the latter equation, we can see that this additional hypothesis means that Bernoulli's law holds underneath the paddle:

$$p + 1/2u^2 = B = \text{constant} = h_N + 1/2u_N^2 = h_L + 1/2u_L^2 \tag{26}$$

because the pressure is hydrostatic at X_N and L.

Physically, it also amounts to neglecting the temporal dependence of the fluid variables under the paddle. i.e. the flow is in a quasi-steady state under the paddle. That is to say that the time to pass under the paddle is smaller that the time of change of velocity.

Note that the equality (26) takes the compact form:

$$\frac{q_L^2}{2h_N^3} = \frac{Fr_N^2}{2} = \frac{\alpha^2}{\alpha + 1} > 1 \tag{27}$$

where $\alpha = \dfrac{h_L}{h_N}$ is the ratio of depths at the two extremities of the paddle. Fr_N is the Froude number at the end of the paddle and the flow is supercritical.

From the Bernoulli equation (26), the pressure can be written:

$$p = \left(h_N + \frac{{q_L}^2}{2h_N}\right) - \frac{{q_L}^2}{2h} \tag{28}$$

and by integrating to get the total pressure force on the paddle, the equation of motion (25) becomes:

$$I\ddot{\hat{Z}} = -1 + \frac{q_L^{4/3}\mu}{2^{2/3}} F(\alpha) \tag{29}$$

where

$$F(\alpha) = \frac{(\alpha - 1)(\alpha^2 + 1)}{\alpha^{4/3}(\alpha + 1)^{1/3}} \tag{30}$$

3.4 Steady state

The steady state (Q_L, H_L, H_N) is calculated easily:

$$F(\alpha_0) = \frac{2^{2/3}}{Q_L^{4/3}\mu} \tag{31}$$

3.5 Linear stability analysis

We now investigate the linear stability around the steady state. From the equations in the reservoir $(0 < x < L)$:

$$h_t + q_x = 0 \tag{32}$$

$$q_t + (\frac{q^2}{h})_x = -hh_x \tag{33}$$

$$\tag{34}$$

We introduce the perturbations about equilibrium:

$$h = H + h' \quad h_L = H_L + h'_L \text{ and } h_N = H_N + Z'$$
$$q = Q + q'$$
$$Z = Z_0 + Z'$$

where $H(= H_L)$ and $Q(= Q_L)$ denote the stationary state.

The linearized equations are then:

$$h'_t + q'_x = 0 \tag{35}$$

$$q'_t + \frac{2Q}{H} q'_x - \frac{Q^2}{H} h'_x = -Hh'_x \tag{36}$$

which can be combined to give:

$$\left(\partial_t + \frac{Q}{H}\partial_x\right)^2 h' = Hh'_{xx} \tag{37}$$

We look for normal modes with $q' = \tilde{q}e^{-i\omega t}$ and $h' = \tilde{h}e^{-i\omega t}$, where ω is the dimensionless frequency:

$$\left(-i\omega + \frac{Q}{H}\partial_x\right)^2 \tilde{h} = H\tilde{h}_{xx} \tag{38}$$

The solutions take the spatial form, $e^{\lambda x}$, where

$$(-i\omega + \frac{Q}{H}\lambda)^2 - H\lambda^2 = 0 \tag{39}$$

$$\lambda_1 = \frac{i\omega}{\frac{Q}{H} - \sqrt{H}} \quad \text{and} \quad \lambda_2 = \frac{i\omega}{\frac{Q}{H} + \sqrt{H}} \tag{40}$$

Thus $\tilde{q} = A_1 e^{\lambda_1 x} + A_2 e^{\lambda_2 x}$ and $\tilde{h} = A_3 e^{\lambda_1 x} + A_4 e^{\lambda_2 x}$. Because the linear problem can be normalized arbitrarily, we set $A_1 = 1$. The boundary conditions q'=0 at x=0 (no perturbed flow rate) then demand $A_2 = -1$. From the continuity equation (35), we have $i\omega\tilde{h} = \tilde{q}_x$, which gives the coefficients,

$$A_3 = \frac{1}{\frac{Q}{H} + \sqrt{H}} \quad \text{and} \quad A_4 = -\frac{1}{\frac{Q}{H} - \sqrt{H}} \tag{41}$$

By introducing $\beta = \dfrac{Q}{H^{3/2}}$ and $\tilde{\Omega} = \dfrac{\Omega}{(1-\beta^2)}$, where $\Omega = \dfrac{\omega}{\sqrt{H}}$, $q'$and h' are finally written:

$$q' = e^{-i\tilde{\Omega}\beta x} 2i \sin(\tilde{\Omega}x) e^{-i\omega t} \tag{42}$$

$$h' = e^{-i\tilde{\Omega}\beta x} \frac{2\tilde{\Omega}}{\omega} \left[\cos(\tilde{\Omega}x) - \beta i \sin(\tilde{\Omega}x)\right] e^{-i\omega \hat{t}} \tag{43}$$

In the same way, we can linearize the equation of the paddle and the Bernoulli equation. Given $h_L = H_L + h'_L$ and $h_N = H_N + Z'$, we have $\alpha = \alpha_0 + \alpha'$ with $\alpha' = \dfrac{h'_L - \alpha_0 Z'}{H_N}$. Then the two linearized equations are:

$$-\omega^2 I Z' = \frac{4}{3}\frac{\mu}{2^{2/3}} Q^{1/3} q'_L F(\alpha_0) + \frac{\mu}{H_N}\frac{F'(\alpha_0)}{F(\alpha_0)}(h'_L - \alpha_0 Z') \tag{44}$$

$$Q q'_L - h'_L H_N^2 \frac{\alpha_0(\alpha_0+2)}{(\alpha_0+1)^2} = \frac{H_N^2 \alpha_0^2 Z'(2\alpha_0+1)}{(\alpha_0+1)^2} \tag{45}$$

where $F'(\alpha_0) = \dfrac{dF}{d\alpha}(\alpha_0)$.

At $x = L$ (with $\xi = l$), the flow rate and the height in the reservoir must be continuous to those in the paddle area (q_L, h_L), so the matching conditions are

$$q_L = q(x = 1 + R\ l(t), t) \tag{46}$$

Using the approximation that R is small, we find

$$q_L \approx q(x = 1, t) \tag{47}$$

In the same way, we have for the perturbed variables:

$$q'_L = q'(x = 1 + R\ l(t), t) \approx q'(x = 1, t) \tag{48}$$

and also $h'_L \approx h'(x = 1)$

Finally, the Bernoulli equation in combination with the equation of the paddle, plus the matching conditions, furnishes an equation of the form, $D(\omega; \alpha_0, I, \mu, Q, H) = 0$, which allows us to determine ω, and where

$$\begin{aligned} D(\omega) = \cos\left(\frac{\Omega}{1-\beta^2}\right)\left[3(1+\alpha_0)F'(\alpha_0) - (2+\alpha_0)\frac{\Omega^2 I}{\mu^2}\left(\frac{\alpha_0+1}{\alpha_0^2}\right)^{2/3}\right] \\ - i\sin\left(\frac{\Omega}{1-\beta^2}\right)\left[\sqrt{2\alpha_0}(1+\alpha_0)^{3/2}(1-\beta^2)\left(F'(\alpha_0) - \frac{2}{3}\frac{2\alpha_0+1}{\alpha_0+1}\frac{F'(\alpha_0)}{\alpha_0\mu} - \frac{\Omega^2 I}{\mu^2}\left(\frac{\alpha_0+1}{\alpha_0^2}\right)^{2/3}\right)\right. \\ \left. + 3\left(\frac{2(1+\alpha_0)}{\alpha_0}\right)^{1/2} F'(\alpha_0) - (\alpha_0+2)\frac{\Omega^2 I}{\mu^2}2^{1/2}\frac{(\alpha_0+1)^{1/6}}{\alpha_0^{11/6}}\right] \end{aligned} \tag{49}$$

The solutions $\omega = \omega_\mathrm{r} + i\ \omega_\mathrm{i}$ can be found numerically. In our convention, modes grow when $\omega_\mathrm{i} > 0$.

3.6 Approximation of small flow rate: $Q \ll 1$ or $\alpha_0 \gg 1$

If the flow rate is small, i.e. $\alpha_0 \gg 1$, then $F(\alpha_0) \sim \alpha_0^{4/3}$ and by keeping the leading order in α_0 in $D(\omega) = 0$, we find $\Omega \approx n\pi$. i.e. in dimensional variables:

$$\omega = n\pi\frac{\sqrt{gH_L}}{X} \tag{50}$$

These are the frequencies of the seiche modes of the reservoir in the absence of the fluid flow.

Proceeding further, and setting $\Omega = n\pi + \gamma$, we find

$$\gamma = \frac{i(1 - \frac{n^2\pi^2 I}{4\alpha_0\mu})}{\frac{1}{3}\alpha_0\sqrt{2}(-1 + \frac{1}{\mu} + \frac{3n^2\pi^2 I}{4\mu^2\alpha_0})} \tag{51}$$

Thus, since the right-hand side of this relation can become positive, the seiche modes can be destablized by the flow. Figure 5 shows the numerical results calculated with experimental parameters and highlights the growth of the instability for the mode $n = 1$.

Thus, the model predicts the existence of flow-destabilized seiches modes. We now follow on and present experimental observations of this phenomenon.

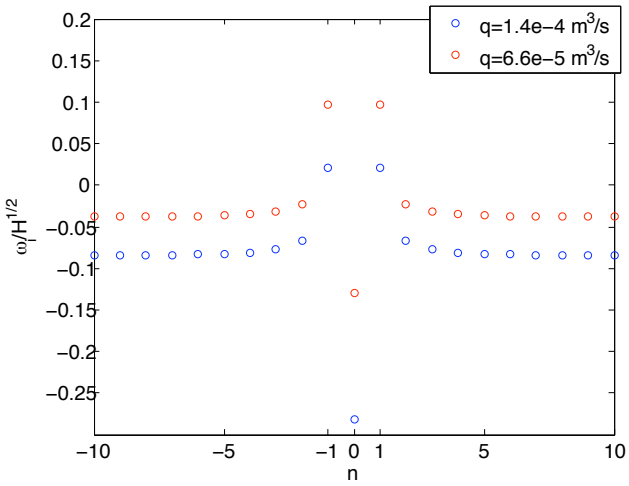

Figure 5: Numerical results: $m_{\text{added}} = 3.1$ g, $x = 5$ cm, $X = 18$ cm, $\theta = 60°$, $H_L \approx 2$ cm.

4 Experimental results

4.1 Steady state

To begin, we explored steady flow states and made measurements of the water depth under the paddle for different masses added on the paddle. These measurements could then be compared with the theoretical ratio α_0 given by the inversion of equation (31). The results, shown in figure 6 (left), reveal agreement between experiment and theory for small masses, but an increasing discrepancy for masses bigger than around 40 g.

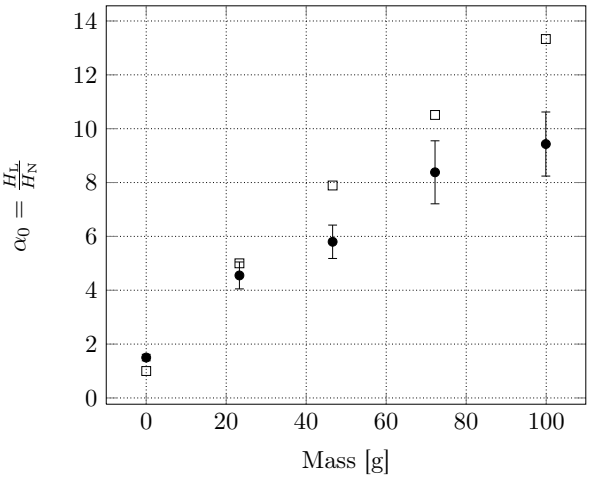

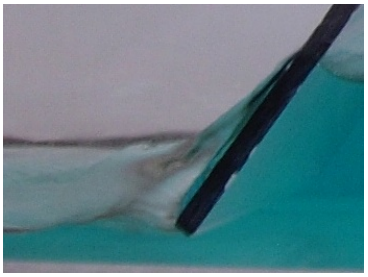

Figure 6: Left: Comparison between experimental points (dots) and numerical calculation using the inversion of $F(\alpha_0) = \frac{2^{2/3}}{Q_L^{4/3}\mu}$ (squares). The angle was fixed at $\theta = 30°$ and $q = 1.6 \times 10^{-4}$ m^3/s. Right: Flow around the paddle instead of underneath in cases of large mass added.

We explain this discrepancy with an observed change of structure in the flow depending

on the value of the mass added on the paddle: for small mass, the fluid flows largely underneath the paddle (as supposed in our model), whereas for large mass, much fluid is also diverted around the sides of the paddle, as illustrated in figure 6 (right).

4.2 Experimental unstable modes

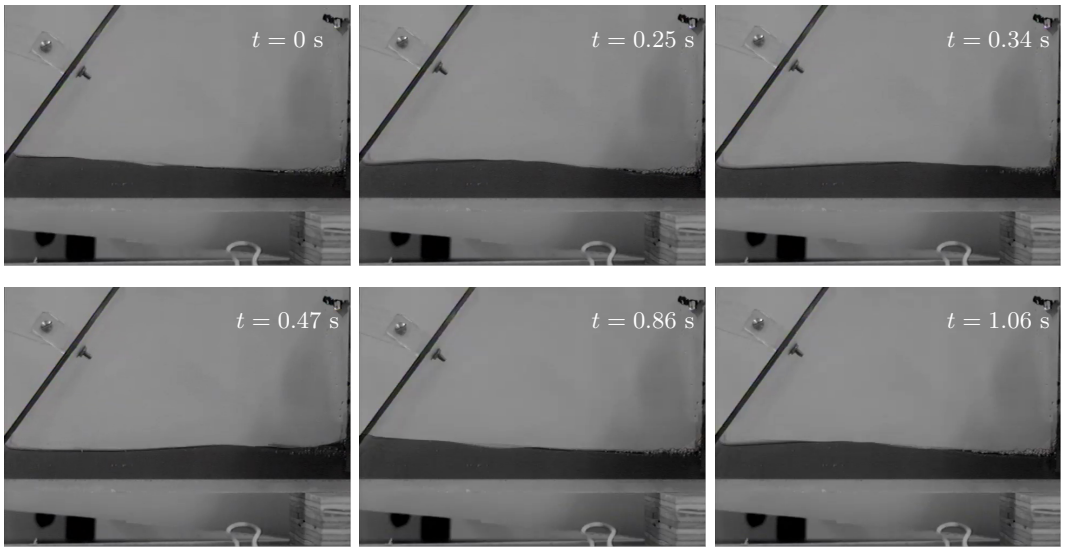

Figure 7: Series of images showing the presence of a flow-destabilized seiche mode n=1 during a period. Experiment with $m_{\text{added}} = 3.1$ g at 5 cm of the pivot.

Figure 7 shows images from an experiment in which a flow-destabilized sloshing mode appeared. From such images, the water level could be extracted by applying a threshold to the intensity of the picture. A time series of the water surface measured in this way is shown in figure 8.

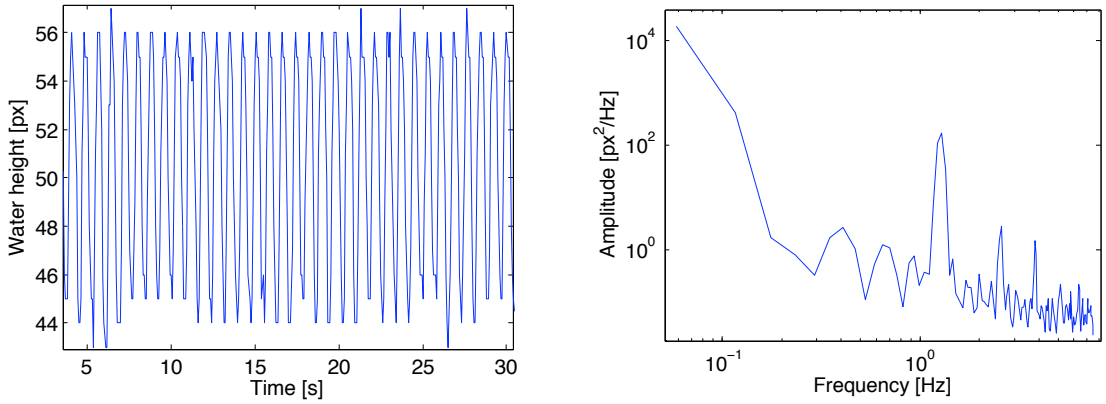

Figure 8: Time series and spectrum for the same experiment as in figure 7.

A comparison between the experiment and the linear theory was made by superimposing the interface observed experimentally with theoretical results using (52):

$$h'(x,t) = e^{-i(\omega t - \tilde{\Omega}\beta x)} \ \frac{2\tilde{\Omega}}{\omega} cos(\tilde{\Omega}x) \quad \text{for } n = 1 \tag{52}$$

On figure 9, the red line corresponds to the theory, with the variables Ω, β and ω calculated from the experimental parameters, except the amplitude and the phase, which were fit using a least squares algorithm.

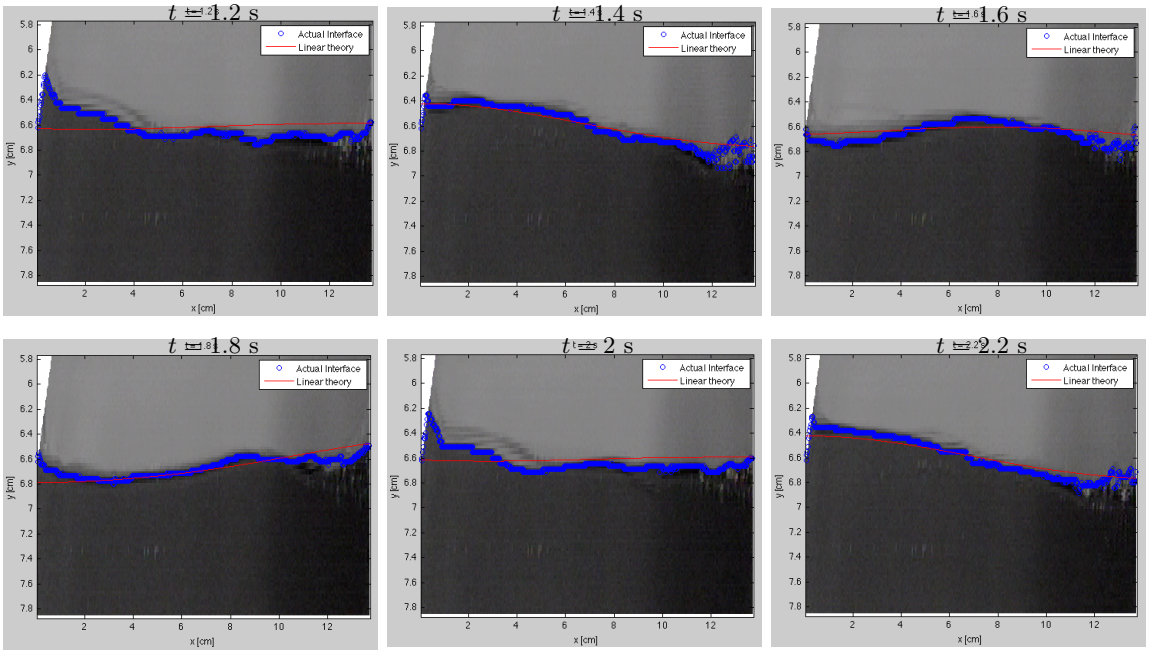

Figure 9: Comparison of the experiment and the linear theory.

Even though the theoretical predictions do not follow exactly the actual interface, especially near the paddle and the wall at the right (where some new elements of physics, like surface tension, should probably be added for a complete description), there is a fair agreement overall, since the main features of the sloshing mode $n = 1$ are well captured.

Higher-order modes with $n = 2$ and 3 were also observed in the experiments. However, it appears that the $n = 1$ mode was usually dominant, probably because the other modes are more strongly damped due to fluid viscosity and friction in the pivot.

4.3 Variations of parameters

After demonstrating the existence of unstable modes, we attempted to further investigate the characteristics of the system by changing control parameters. Figure 10 presents the frequency of the paddle oscillations for masses placed at different positions on the rod (left) and varying flow rate (right).

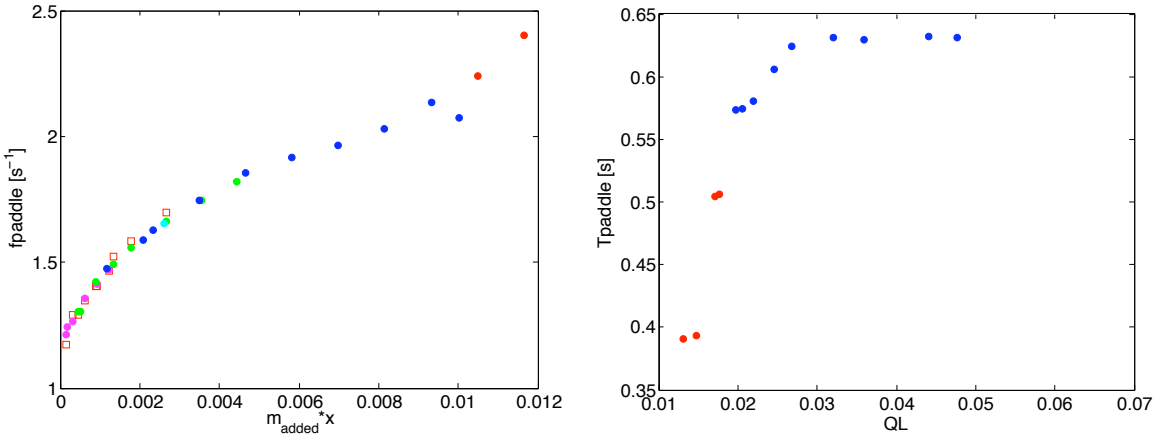

Figure 10:
Left: Variation of m_{added} at q fixed. ($q = 1.42 \times 10^{-4}$ m^3/s). Each colour represents one series of experiments realized with one particular m_{added} translated at different positions on the rod. The frequency of the paddle motion has been measured with a stopwatch (looking at 50 oscillations). For checking, the square points are the frequency of the paddle determined using the spectrum of the time series of the water level (like in figure 8) for some experiments.
Right: Variation of q at m_{added} fixed. ($m_{added} = 8.9$ g and $x = 25$ cm). See also section 4.4.2.

4.4 Evidence of non-linearities

4.4.1 Beating

In certains experiments, the water level was characterized by a beating motion, as illustrated in figure 11. Though beating is not itself a non-linear phenomenon, the spectrum reveals a possible resonant triad with the superposition of two frequencies (the main frequency and another one smaller) which creates the two additional peaks around the main peak and its harmonics.

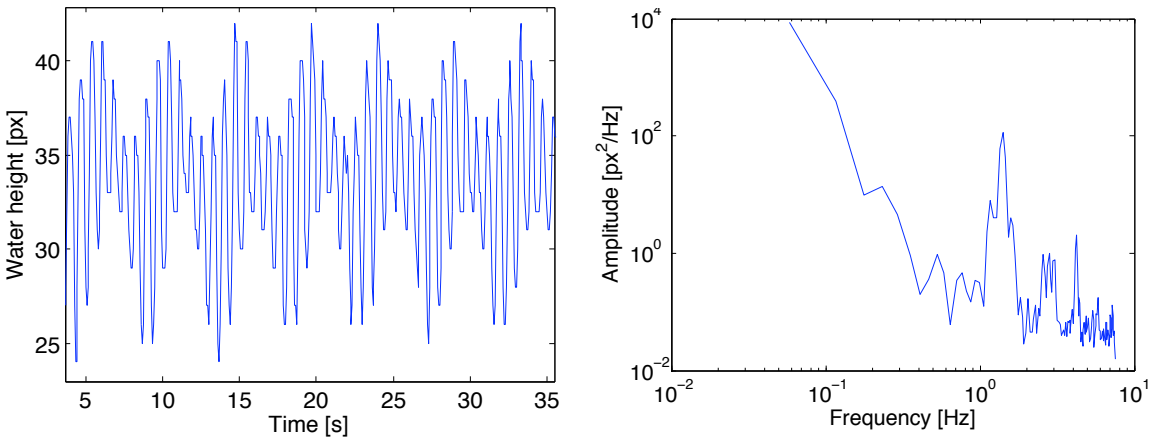

Figure 11: Time series and spectrum for $m_{\text{added}} = 3.1$ g at 30 cm of the pivot.

4.4.2 Bistability

Another observed feature typical of a non-linear behaviour is bistability: in some experiments, the unstable behaviour could be stopped by gently bringing the paddle to rest with one's hand; after being released the paddle remained stationary and no instability grew. At the same time, by giving a little kick to the paddle, the flow-destabilized sloshing could be resumed. Thus, for the same set of parameters, the system could be both in a steady or sloshing regime. On the other hand for other ranges of parameters, the system was only unstable (see figure 12).

The existence of bistability suggests that the system could follow a subcritical bifurcation, as sketched in figure 12 (right). The limit between the bistable regime and unstable regime can then be considered as the linear threshold of the instability.

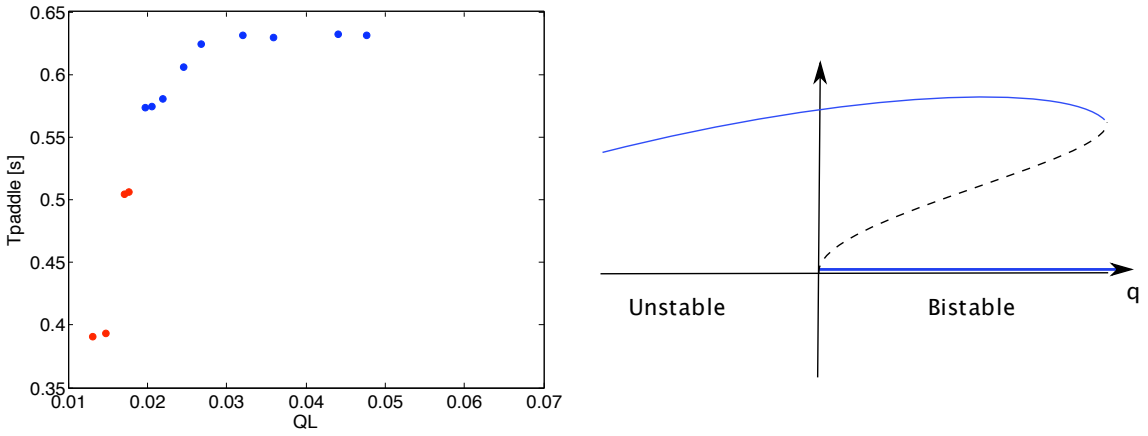

Figure 12: Presence of bistability: ●: unstable points. ●: bistable points. Right: Subcritical bifurcation.

5 Conclusion

The phenomenon of flow-destabilized sloshing modes has been demonstrated experimentally with a setup analogous to a water clarinet'. The linear theory shows some agreement with the experimental unstable modes.

However, several limits of the model can be pointed out. It does not take into account water flow around the sides of the paddle. Friction in the hinge has been neglected, together with fluid viscosity and surface tension. The experiment also sometimes suggests a possible collision of the paddle with the bottom, an interaction not included in the model. We can also question the validity of the shallow water hypothesis and the Bernoulli approximation under the paddle for the experimental conditions.

Finally, experiments reveal that work must be done to go beyond linear theory in order to capture the observed non-linear dynamics like resonant triad and bistability.

6 Acknowlegments

I would like to thank my supervisor Neil Balmforth for all his help and ideas, together with Bill Young for his help in the first calculations and Andrew Belmonte for his advice in the experimental setup. I am also very grateful to Roger Grimshaw and Harvey Segur for their very good lectures on non-linear waves. Finally, I thank all the fellows and the staff for the pleasant atmosphere during the whole summer at Walsh Cottage.

References

[1] J. Backus, *Small-vibration theory of the clarinet*, The Journal of the Acoustical Society of America, 35 (1963), pp. 305–313.

[2] B. J. Binder and J.-M. Vanden-Broeck, *Free surface flows past surfboards and sluice gates*, European Journal of Applied Mathematics, 16 (2005), pp. 601–619.

[3] J.-P. Dalmont, J. Gilbert, J. Kergomard, and S. Ollivier, *An analytical prediction of the oscillation and extinction thresholds of a clarinet*, The Journal of the Acoustical Society of America, 118 (2005), pp. 3294–3305.

[4] M. E. McIntyre, R. T. Schumacher, and J. Woodhouse, *On the oscillations of musical instruments*, The Journal of the Acoustical Society of America, 74 (1983), pp. 1325–1345.

[5] A. C. Rust, N. Balmforth, and S.Mandre, *The feasibility of generating low-frequency volcano seismicity by flow through a deformable channel*, Geological Society, London, Special Publications, 307 (2008), pp. 45–56.